Analysis of the imaging method for assessment of the smile of laser diode bars

Luis Martí-López,[1,*] José A. Ramos-de-Campos,[2] and Walter D. Furlan[3]

[1]Centro de Aplicaciones Tecnológicas y Desarrollo Nuclear, Calle 30 esq. 5ta Avenida, Playa, La Habana, Cuba

[2]Instituto Tecnológico de Óptica, Color, e Imagen, Nicolás Copérnico 7–13. Parque Tecnológico de Valencia, 46980 Valencia, Spain

[3]Departamento de Óptica, Universidad de Valencia, 46100 Burjasot, Valencia, Spain

*Corresponding author: marti@ceaden.edu.cu

Received 30 September 2008; revised 21 July 2009; accepted 10 August 2009; posted 11 August 2009 (Doc. ID 102162); published 1 September 2009

We study imaging systems designed to assess the smile of laser diode bars (LDBs). The magnification matrix is derived from the required sampling period and the geometries of the LDBs and the charge-coupled device (CCD) array. These image-forming systems present in-plane pure translation invariance, but in the case of anamorphic ones, lack in-plane rotation invariance. It is shown that the smile parameters of the image of the LDB are linked with the smile parameters of the LDB by simple mathematical expressions. The spatial resolution of such optical systems is estimated at approximately 1 μm for a mean wavelength of $\lambda \approx 800$ nm. Our results suggest that, with the current state-of-the-art, the formation of imaging methods for LDB smile assessment can be used to assess smile heights $\geq 1\,\mu$m. © 2009 Optical Society of America

OCIS codes: 140.2010, 120.4640, 110.2960.

1. Introduction

Laser diode bars (LDBs) are composed of many laser diodes (LDs) aligned in a straight row [1,2]. In real LDBs the LDs are not perfectly aligned because of technical limitations of the manufacturing process. This defect appears as a curvature of the line of LDs and is called smile [2–4]. The smile reduces the performance of the optical systems employed for shaping, delivery, transformation, and focusing of laser beams emitted by LDBs [3]. This circumstance stimulates the efforts to improve mounting technologies and to develop methods to assess the smile of LDBs. Three methods for characterization of the smile of LDBs have been reported:

The imaging method (IM). An image of the LDB is captured by a charge-coupled device (CCD) array, digitized, stored, and processed in a personal computer (PC). Images of LDB smiles have appeared in many articles; see, for example, [2,4–7]. The main use of the IM is for qualitative description of the smile.

The near-field scanning optical microscopy (NSOM) method [8,9]. The distal tip of an optical fiber is scanned over the output facet of the LDB. The captured laser radiation is delivered by the optical fiber to a photoelectric detector, which converts it into an electrical signal, which in turn is digitized, stored, and processed in a PC. The data of positions and LDB radiation can be employed to derive a map of the radiant emission of the facet of the LDB and to characterize the smile; see [10,11].

The interferometric method in a Lloyd's mirror setup. The LDB is placed in a Lloyd's mirror setup, and the interference fringes are captured by a CCD array, digitized, stored, and processed in a PC. The parameters of the smile are derived from the stored data [12].

The IM is the simplest and most often used method for smile characterization. However, to the best of

0003-6935/09/264880-05$15.00/0

our knowledge, no detailed study of its properties and limitations has been reported. In contrast, both the NSOM and the interferometric methods have been reported in the literature [8–12]. Our goal here is to discuss some basic features of the IM for LDB smile characterization. In Section 2 we define the smile height (SH), the smile aspect ratio (SAR), and the smile parameter S, which are employed later to analyze the influence of the imaging system on their characterization. In Section 3 we describe the imaging systems for LDB smile assessment. In Section 4 the relations that link the LDB smile parameters with analogous parameters measured in its image are derived. In Section 5 we present our conclusions.

2. Smile Parameters

Figure 1 shows the output facet of a LDB composed of N LDs, numbered from $q = 1$ to $q = N$. The LDB is framed within a rectangle of sides $L \times \mathrm{SH}$, where L is the length of the LDB and SH is the distance between the outer LDs, measured in the direction perpendicular to the LDB. Now we define the smile aspect ratio (SAR) as

$$\mathrm{SAR} = \frac{\mathrm{SH}}{L}, \tag{1}$$

The typical values of SH and L are $0 \le \mathrm{SH} \le 10\,\mu\mathrm{m}$ and $L \ge 10\,\mathrm{mm}$. Therefore, the SAR varies from 0 (for a LDB with no smile) to approximately 10^{-3}.

Figure 2 shows another scheme of the output facet of a LDB. The AA' line represents the straight line that best fits the position of the LDs of the LDB. The position of the qth LD on the plane of the output facet is (ξ_q, η_q). We define smile parameter S of a LDB as [12]

$$S = \sqrt{\frac{1}{N}\sum_{q=1}^{N} \delta_q^2}, \tag{2}$$

where δ_q is the distance from the qth LD to segment AA' and $N > 2$ is the number of LDs. Parameter S ranges from $0\,\mu\mathrm{m}$ (for a LDB with no smile) to a few micrometers. Further we assume that, in a good approximation, Eq. (2) can be rewritten as

$$S = \sqrt{\frac{1}{N}\sum (b\xi_q + d - \eta_q)^2}, \tag{3}$$

where b and d are the slope and the intercept, respectively, of line AA' obtained by a least-squares fit of the function

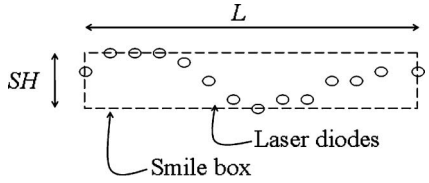

Fig. 1. Scheme of a LDB smile; each ellipse represents the active zone of a LD.

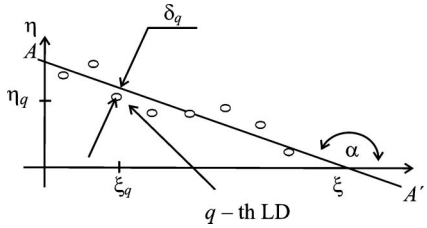

Fig. 2. Coordinate system and variables at the output facet of the LDB. Each ellipse represents the active zone of a LD.

$$\eta = b\xi + d \tag{4}$$

and can be calculated using the expressions:

$$b = \frac{\langle \xi_q \eta_q \rangle + \langle \xi_q \rangle \langle \eta_q \rangle}{\langle \xi_q^2 \rangle - \langle \xi_q \rangle^2}, \tag{5}$$

$$d = \langle \eta_q \rangle - b\langle \xi_q \rangle, \tag{6}$$

where

$$\langle \xi_q^2 \rangle = \frac{1}{N}\sum_{q=1}^{N} \xi_q^2, \tag{7}$$

$$\langle \xi_q \rangle = \frac{1}{N}\sum_{q=1}^{N} \xi_q, \tag{8}$$

$$\langle \eta_q \rangle = \frac{1}{N}\sum_{q=1}^{N} \eta_q, \tag{9}$$

$$\langle \xi_q \eta_q \rangle = \frac{1}{N}\sum_{q=1}^{N} \xi_q \eta_q. \tag{10}$$

Thus, parameter S describes the smile geometry by use of a statistical procedure. Note that in-plane pure translations and in-plane rotations of the LDB do not alter the values of SH, SAR, and S.

3. Main Properties of the Imaging Method

In the IM for smile characterization an image of the LDB is formed by an optical system on a scientific grade CCD array. The CCD captures the image, converts it into an electrical signal, which in turn is digitized and transformed into an irradiance matrix in an image acquisition block. This irradiance matrix is saved in a PC, where it can be digitally processed at a later time. A block diagram of the setup is shown in Fig. 3(a); Fig. 3(b) shows a simplified scheme of a CCD array. Typical scientific grade CCD arrays have $M \times Q$ pixels, for example, 128×1024, 2048×2048, or 4096×4096 pixels, a pixel period of $T \approx 5$–$15\,\mu\mathrm{m}$ (sampling period), and side lengths $a, b \approx 12$–$60\,\mathrm{mm}$. This means that the shape of the LDB, the shape and the pixel period of the CCD array, and the Whittaker–Shannon sampling theorem [13,14]

impose specific design requirements on the optical system.

Let us suppose that the SH ranges from 1 to 10 μm and that the CCD pixel period is 15 μm. We then need a magnification of 8–15× to attain a spatial sampling period of 1–2 μm in the object plane; to achieve a spatial sampling period of 0.2–0.3 μm (which is, of course, a better sampling) we need a magnification of 30–50×. If the optical system has the same magnification in both axes, the image in the direction parallel to the LDB may be too large. Consider, for example, a 10 mm long LDB. Its image is 80 mm long for a magnification of 8× and 500 mm long for a magnification of 50×. Consequently, in most cases the length of the image of the LDB exceeds the length of the CCD array. To avoid this inconvenience, the optical system is designed so that the magnification in the direction perpendicular to the LDB is larger than the magnification in the direction parallel to it. Consequently, the optical system stretches the image in the direction perpendicular to the LDB. In other words, the image is anamorphic. This feature of the image is reminiscent of the portraits by the great Italian painter and sculptor, Amadeo Modigliani (1884–1920). For a review on anamorphic images see [15].

It should be pointed out that in some cases there is no need for an anamorphic optical system. For example, a nonanamorphic 3× magnification well-corrected optical system with a numerical aperture of ≈0.5 (*f*/No. ≈ 2), combined with a CCD array of $T \approx 5\,\mu$m and side lengths of $a \approx 37.5$ mm and b ≈ 5 mm is suitable for characterization of a 10 mm length LDB with a SH of ≈ 10 μm.

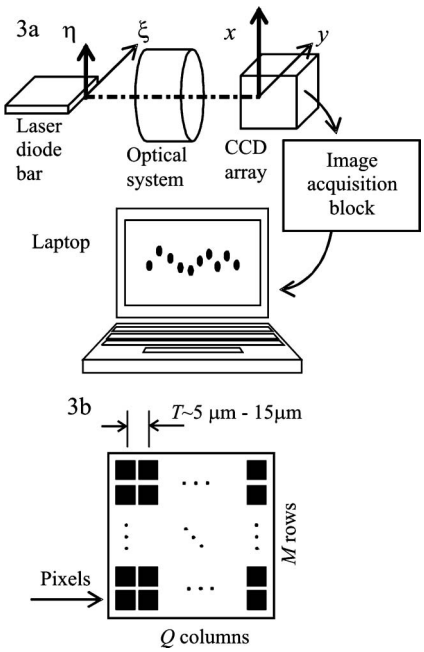

Fig. 3. Block diagram of the setup of the IM for smile assessment: (a) simplified block diagram of the setup and (b) scheme of the CCD array.

Now consider an ideal optical system that forms an image of the output facet of the LDB on the CCD array. The planes of the output facet of the LDB and of the CCD array are normal to the optical axis, which means that there is no perspective distortion. This optical system maps a point $\mathbf{r} = (\xi, \eta)$ of the object plane onto a point $\mathbf{r}' = (x, y)$ of the image plane, according to the expression

$$\mathbf{r}' = \mathbf{M}\mathbf{r}, \tag{11}$$

where $\mathbf{M}$ is the magnification matrix:

$$\mathbf{M} = \begin{bmatrix} m_x & 0 \\ 0 & m_y \end{bmatrix}, \tag{12}$$

where m_x and m_y have the same sign. When magnifications m_x and m_y are adequately chosen, the image of the LDB fits the CCD array. If $m_x \neq m_y$, the optical system is anamorphic.

A. Translation invariance

Consider two arbitrary points O_1 and O_2 of the object with coordinates $\mathbf{r}_1 = (\xi_1, \eta_1)$ and $\mathbf{r}_2 = (\xi_2, \eta_2)$, respectively. The optical system projects points O_1 and O_2 on the image plane. The corresponding image points are P_1 and P_2 with coordinates $\mathbf{r}'_1 = (x_1, y_1)$ and $\mathbf{r}'_2 = (x_2, y_2)$, respectively. Object vector

$$\Delta\mathbf{r} = \mathbf{r}_2 - \mathbf{r}_1 \tag{13}$$

is projected onto the image plane, with the vector

$$\Delta\mathbf{r}' = \mathbf{r}'_2 - \mathbf{r}'_1 \tag{14}$$

as the corresponding image vector. Applying the linear transformation in Eq. (11) we obtain

$$\Delta\mathbf{r}' = \mathbf{M}\Delta\mathbf{r}. \tag{15}$$

Consider now an in-plane pure translation of the object $\mathbf{t}$, so that the new positions of object points O_1 and O_2 are $\mathbf{r}_1 + \mathbf{t}$ and $\mathbf{r}_2 + \mathbf{t}$, respectively. This transformation yields the image vector $\Delta\mathbf{r}'_{\text{new}}$:

$$\Delta\mathbf{r}'_{\text{new}} = \mathbf{M}(\mathbf{r}_2 + \mathbf{t}) - \mathbf{M}(\mathbf{r}_1 + \mathbf{t}). \tag{16}$$

It is obvious that

$$\Delta\mathbf{r}'_{\text{new}} = \Delta\mathbf{r}'. \tag{17}$$

Therefore, in-plane pure translations of the object do not alter the shape of its image. This conclusion is valid for ideal imaging systems; in real optical systems, aberrations limit the validity of this result.

B. Rotation Invariance

Consider again two arbitrary points O_1 and O_2 of the object with coordinates $\mathbf{r}_1 = (\xi_1, \eta_1)$ and $\mathbf{r}_2 = (\xi_2, \eta_2)$, respectively. The corresponding image points are P_1 and P_2 with coordinates $\mathbf{r}'_1 = (x_1, y_1)$ and $\mathbf{r}'_2 = (x_2, y_2)$, respectively. The object vector in Eq. (14) can be rewritten as

$$\Delta \mathbf{r} = |\Delta \mathbf{r}| \begin{bmatrix} \cos\theta \\ \sin\theta \end{bmatrix}, \tag{18}$$

where θ is the angle between vector $\Delta\mathbf{r}$ and the ξ axis. Notice that the parameter θ describes the in-plane rotation of vector $\Delta\mathbf{r}$ and that the modulus of vector $\Delta\mathbf{r}$ does not depend on θ.

Applying Eq. (16) we find the projection of vector $\Delta\mathbf{r}$ on image plane $\Delta\mathbf{r}'$:

$$\Delta \mathbf{r}' = \mathbf{M}|\Delta \mathbf{r}| \begin{bmatrix} \cos\theta \\ \sin\theta \end{bmatrix}. \tag{19}$$

Accordingly, the modulus of vector $\Delta\mathbf{r}'$ and its angle β with respect to the x axis for $|\theta| < \pi/2$ are

$$|\Delta \mathbf{r}'| = |\Delta \mathbf{r}| \sqrt{m_x^2 \cos^2\theta + m_y^2 \sin^2\theta}, \tag{20}$$

$$\tan\beta = \frac{m_y}{m_x} \tan\theta. \tag{21}$$

If the optical system is anamorphic, from Eqs. (20) and (21) it follows that the modulus and direction of vector $\Delta\mathbf{r}'$ depend on θ and, consequently, the image is not rotation invariant. In addition, vector $\Delta\mathbf{r}'$ is parallel to $\Delta\mathbf{r}$ only for $\theta = 0$.

For an anamorphic optical system the image shape depends on the angular alignment of the LDB with respect to the x axis, which is illustrated in Fig. 4. This means that we must determine the relation between the smile parameter in the image plane and the smile parameter in the object plane, as will be shown in Section 4.

C. Spatial Resolution

For SHs ranging from 1 to 10 μm the required spatial resolution is approximately 1 μm or better. Note that this spatial resolution is comparable with the spatial resolution of dry optical microscopes. As with any optical system for microscopy, the spherical aberration, coma, field curvature, and distortion must be significantly corrected. The chromatic aberration is not a problem because the spectral bandwidth of the LDs is narrow.

We now consider that LDs are incoherent with respect to each other and that the aperture in the fast axis is determined by the optical system. Applying the expression of the spatial resolution for incoherent light [16] to estimate the spatial resolution in fast axis R in air we obtain

$$R \sim \frac{0.5\lambda}{\mathrm{NA}}, \tag{22}$$

where λ is the mean wavelength and NA is the numerical aperture of the optical system. Assuming $\lambda \approx 800$ nm and a NA of ≈ 0.5 (f/No. ≈ 2), we obtain $R \approx 800$ nm. Therefore, the IM seems to work well for a SH >1 μm (for $\lambda \approx 800$ nm). By use of better optical objectives (with a larger aperture) and digital image processing such resolution can be improved substantially; see, for example, [16,13].

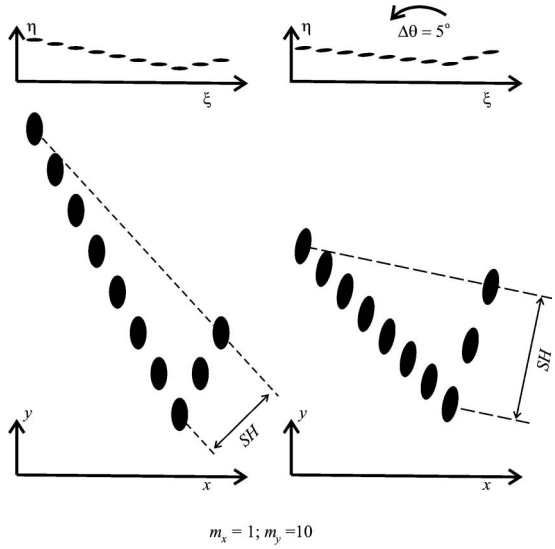

Fig. 4. Image LDB smile variation that is due to rotation for $m_x = 1$, $m_y = 10$. (a) Simulated LDB and corresponding image. (b) The same simulated LDB with an in-plane counterclockwise rotation of $\Delta\theta = 5°$ and the resulting image. Note the change in the SH of the image.

4. Transformation of Smile Parameters

A. Smile Height and Smile Aspect Ratio

The smile height, SH′, length L', and the smile aspect ratio, SAR′, of the LDB image are linked with the corresponding parameters in the object plane, SH, L, and SAR by the expressions

$$\mathrm{SH}' = \mathrm{SH} \sqrt{m_x^2 \cos^2\gamma + m_y^2 \sin^2\gamma}, \tag{23}$$

$$L' = L \sqrt{m_x^2 \sin^2\gamma + m_y^2 \cos^2\gamma}, \tag{24}$$

$$\mathrm{SAR}' = \frac{\sqrt{m_x^2 \cos^2\gamma + m_y^2 \sin^2\gamma}}{\sqrt{m_x^2 \sin^2\gamma + m_y^2 \cos^2\gamma}} \mathrm{SAR}, \tag{25}$$

where γ is the angle between segment HH' and axis ξ. Proof of the above expressions is straightforward. For $\gamma \approx \pi/2$, $\sin^2\gamma \approx 1$, and $\cos^2\gamma \approx 0$, Eqs. (23)–(25) transform into

$$\mathrm{SH} = |m_y| \mathrm{SH}, \tag{26}$$

$$L' = |m_x| L, \tag{27}$$

$$\mathrm{SAR}' = \frac{m_y}{m_x} \mathrm{SAR}. \tag{28}$$

B. Smile Parameter

Slope b' and intercept on the y axis d' of the least-squares straight line that fits image points (x_q, y_q), $q = 1, 2, \ldots, N$, are

$$b' = \frac{\langle x_q y_q \rangle + \langle x_q \rangle \langle y_q \rangle}{\langle x_q^2 \rangle - \langle y_q \rangle^2}, \tag{29}$$

$$d' = \langle y_q \rangle - b' \langle x_q \rangle, \tag{30}$$

where

$$\langle x_q^2 \rangle = \frac{1}{N} \sum_{q=1}^{N} x_q^2, \tag{31}$$

$$\langle x_q \rangle = \frac{1}{N} \sum_{q=1}^{N} x_q, \tag{32}$$

$$\langle y_q \rangle = \frac{1}{N} \sum_{q=1}^{N} y_q, \tag{33}$$

$$\langle x_q y_q \rangle = \frac{1}{N} \sum_{q=1}^{N} x_q y_q, \tag{34}$$

Applying Eq. (13) to Eqs. (31) and (32) we obtain

$$b' = \frac{m_y}{m_x} b, \tag{35}$$

$$d' = m_y d. \tag{36}$$

We now calculate the smile parameter in the image of the DB, S'. After a straightforward calculation we obtain

$$S' = |m_y| S. \tag{37}$$

5. Conclusions

We introduced a set of parameters, namely, the smile height (SH), the smile aspect ratio (SAR), and the smile parameter S, to characterize the smile of LDBs. We then derived the form of the magnification matrix taking into account the required sampling period and geometry factors. We showed that anamorphic optical systems present in-plane pure translation invariance but lack rotation invariance. Analysis of the spatial resolution strongly suggests that the IM works well for LDBs with a SH $\geq 1\,\mu$m. We demonstrated that the smile parameters of the image of the LDB are linked with the smile parameters of the LDB by simple mathematical expressions. It should be pointed out that some reported optical systems for smile characterization present perspective distortion. For example, an optical setup with a CCD camera located off axis as in Ref. [7] introduces one-dimensional perspective distortion in the image. In practice, perspective distortion is undesirable and a careful alignment is done to avoid it.

Overall our analysis suggests that the IM for LDB smile assessment in its current state-of-the-art works well for smile heights $\geq 1\,\mu$m for $\lambda \approx 800$ nm and a NA of ≈0.5 (*f*/No. ≈ 2). Better objectives and the use of digital processing are needed for assessment of small smiles ($0 \leq \mathrm{SH} < 1\,\mu$m).

We are indebted to anonymous reviewers for their constructive criticism that contributed to the improvement of this paper. This research was carried out with the support of the Asociación Industrial de Óptica, Color e Imagen (AIDO), Valencia, Spain, and of the Centro de Aplicaciones Tecnológicas y Desarrollo Nuclear (CEADEN), La Habana, Cuba. W. D. Furlan acknowledges financial support from Ministerio de Ciencia y Tecnología, Spain, grant DPI 2008-02953. J. A. Ramos-de-Campos and W. D. Furlan can be contacted by e-mail at jaramos@aido.es and walter.furlan@uv.es, respectively.

References

1. G. A. Agrawal and N. K. Dutta, *Semiconductor Lasers*, 2nd ed. (Van Nostrand Reinhold, 1993).
2. R. Diehl, *High-Power Diode Lasers: Fundamentals, Technology, Applications* (Springer-Verlag, 2000).
3. H.-G. Treusch, A. Ovtchinnikov, X. He, M. Kanskar, J. Mott, and S. Yang, "High-brightness semiconductor laser sources for materials processing: stacking, beam shaping, and bars," IEEE J. Sel. Top. Quantum Electron. **6**, 601–614 (2000).
4. W. Schulz and R. Poprawe, "Manufacturing with novel high-power diode lasers," IEEE J. Sel. Top. Quantum Electron. **6**, 696–705 (2000).
5. N. U. Wetter, "Three-fold effective brightness increase of laser diode bar emission by assessment and correction of diode array curvature," Opt. Laser Technol. **33**, 181–187 (2001).
6. C. L. Talbot, M. E. J. Friese, D. Wang, I. Brereton, N. R. Heckenberg, and H. Rubinsztein-Dunlop, "Linewidth reduction in a large-smile laser diode array," Appl. Opt. **44**, 6264–6268 (2005).
7. J. F. Monjardin, K. M. Nowak, H. J. Baker, and D. R. Hall, "Correction of beam errors in high power laser diode bars and stacks," Opt. Express **14**, 8178–8183 (2006).
8. U. Dürig, D. W. Pohl, and F. Rohner, "Near field optical-scanning microscopy," J. Appl. Phys. **59**, 3318–3327 (1986).
9. E. Betzig and J. K. Trautman, "Near-field optics: microscopy, spectroscopy, and surface modification beyond the diffraction limit," Science **257**, 189–195 (1992).
10. W. D. Herzog, M. S. Ünlü, B. B. Goldberg, G. H. Rodees, and C. Harder, "Beam divergence and waist measurements of laser diodes by near-field scanning optical microscopy," Appl. Phys. Lett. **70**, 688–690 (1997).
11. C. Scholz and M. Belitz, "High resolution near-field analysis of high-power diode lasers," http://www.ilt.fraunhofer.de/eng/100299.html.
12. L. Martí-López, J. A. Ramos-de-Campos, and R. A. Martínez-Celorio, "Interferometric method for characterizing the smile of laser diode bars," Opt. Commun. **275**, 359–371 (2007).
13. M. S. Nixon and A. S. Aguado, *Feature Extraction and Image Processing* (Newnes, 2002).
14. J. W. Goodman, *Introduction to Fourier Optics*, 2nd ed. (McGraw-Hill, 1996).
15. J. L. Hunt, B. G. Nickel, and C. Gigault, "Anamorphic images," Am. J. Phys. **68**, 232–237 (2000).
16. S. Inoué and R. Oldenbourg, "Microscopes," in *Handbook of Optics: Devices, Measurements and Properties,* M. Bass, E. W. Van Stryland, D. Williams, and W. L. Wolfe, eds. (McGraw-Hill, 1995), Vol.2.